Proceedings of the 28th IEEE
EMBS Annual International Conference
New York City, USA, Aug 30-Sept 3, 2006

Bidimensional MRI-based Navigation System Using a PID Controller

Samer Tamaz[1], *Student Member, IEEE-EMBS*, Richard Gourdeau[2], Sylvain Martel[1*], *Member IEEE*

[1]NanoRobotics Laboratory, Department of Computer Engineering and Institute of Biomedical Engineering
École Polytechnique de Montréal (EPM), Campus of the Université de Montréal, Montréal (Québec) Canada
[2]Department of Electrical Engineering
École Polytechnique de Montréal (EPM), Campus of the Université de Montréal, Montréal (Québec) Canada

*E-mail: sylvain.martel@polymtl.ca URL: www.nano.polymtl.ca

Abstract—The feasibility of using 2D real-time control to navigate ferromagnetic entities in an MRI bore for novel medical interventions is assessed. Preliminary experimental results confirm that a simple PID controller can be suitable for several applications where targeting out-of-reach locations within the cardiovascular system is essential.

Keywords—**Feedback motion control, real-time, MRI, time delay, fluid drag, magnetic propulsion, microdevice**

I. Introduction

The goal of the MR-Sub (Magnetic Resonance Submarine) project is to guide and propel a microdevice in the human cardiovascular system using a clinical Magnetic Resonance Imaging (MRI) platform [1]. Among the various applications considered, the MR-Sub is intended for drug delivery through tiny blood vessels as small as capillaries. Studies on propulsion at the macroscale and microscale levels, have been proved to be feasible using the magnetic gradients provided by an upgraded MRI system [2,3,4]. In order to locate the position of the microdevice along its motion, a new real-time tracking technique has been developed [5]. A position feedback controller embedded in the real-time software architecture ensures proper navigation of the untethered device along complex vessel pathways [6]. The itinerary of microdevice is fragmented into rectilinear segments by the attribution of waypoints [7]. A PID controller has been selected for its simplicity while allowing easy identifications of the physiological and technological constraints [8].

II. Modelling

To conduct preliminary experimental tests to validate the use of a clinical MRI system to navigate horizontally and vertically a ferromagnetic core *in vitro*, a simplified model was considered initially. The ferromagnetic spherical bead being navigated through the induction of magnetic gradients generated here by the MR-imaging coils is subjected to five forces. The magnetic force is defined as

$$F_m = V_m \cdot (M \cdot \nabla) B \tag{1}$$

where V_m is the volume of the ferromagnetic entity (here being a bead), M is the magnetization of the ferromagnetic bead, and ∇B is the magnetic gradient amplitude. The drag force acting against the bead is expressed as

$$D = \frac{1}{2} \rho_f \cdot u^2 \cdot A_t \cdot C_D \tag{2}$$

where ρ_f is the fluid density, u is the relative velocity between the bead and the fluid, A_t is the cross-sectional area of the bead, and C_D is the drag coefficient for a sphere defined as

$$C_{D\infty} \approx \frac{24}{\mathrm{Re}} + \frac{6}{1+\sqrt{\mathrm{Re}}} + 0.4\,; \qquad 0 \le \mathrm{Re} \le 2\times 10^5 \cdot \tag{3}$$

In Eq. 3, *Re* is the Reynolds number and it is defined as

$$\mathrm{Re} = \frac{\rho_f . u . d_b}{\mu} \tag{4}$$

where μ is the fluid viscosity, and d_b the diameter of the bead. The infinite sign in Eq. 3 denotes a distance far enough from the bead such that variations of the drag force due to the wall of the vessel is negligible. A constant instead of pulsating fluid speed was also considered initially. The buoyancy force may also have an impact and it is expressed as

$$\mathrm{b} = \mathrm{V} \cdot \rho_f \cdot \mathrm{g} \tag{5}$$

where V is the volume of the bead and g is the gravitational acceleration. The weight of the bead is defined as

$$\mathrm{W} = \mathrm{V} \cdot \rho \cdot \mathrm{g} \tag{6}$$

where ρ is the mass density of the bead. The friction force is defined as

$$\mathrm{f} = \mu\,(\mathrm{W\text{-}b}) \tag{7}$$

with μ being the friction coefficient, which can either be static μ_s or kinetic μ_k.

III. Controller

In order to ensure a rectilinear trajectory along the segments traveled by the ferromagnetic bead for the 2D model being subjected to a quiescent or laminar flow, the commands applied along the x and z axes are determined based on a polar coordinates system. The orientation within the Cartesian system with respect to the MRI bore is depicted in Fig. 1. For control purpose, a discrete PID controller was also selected whose discrete transfer function is expressed by

$$K(z) = \frac{U_T(z)}{E_r(z)} = K_{TP} + K_{TD}\frac{z-1}{zh} + K_{TI}\frac{zh}{z-1}. \qquad (8)$$

In Eq. 8, E_r represents the quadratic distance separating the targeted position of the bead from its current position, U_{Tr} is the magnitude of the command along the r coordinate that acts effectively along the transverse direction of the current segment, with K_{TP}, K_{TD}, and K_{TI} representing the transverse proportional, derivative, and integral gain respectively. The time based error is the quadratic error defined as

$$e_r(t) = \sqrt{\left(x_D - x(t)\right)^2 + \left(z_D - z(t)\right)^2}\ . \qquad (9)$$

The commands along the x and z axes are derived respectively by the following equations

$$\begin{aligned} U_x(z) &= U_{Tr}(z)\cos(\theta) - U_{Nx}(z) \\ U_z(z) &= U_{Tr}(z)\sin(\theta) - U_{Nz}(z) \end{aligned} \qquad (10)$$

Where U_{Nx} and U_{Nz} represent the magnitude of the command along the x and z coordinates respectively that act along the normal direction of the segment as described by the following equations

$$\begin{aligned} U_{Nx}(z) &= K_{NP}E_{Nr}(z)\cos(\alpha) + K_{ND}V_{Nr}(z)\cos(\beta) \\ U_{Nz}(z) &= K_{NP}E_{Nr}(z)\sin(\alpha) + K_{ND}V_{Nr}(z)\sin(\beta) \end{aligned} \qquad (11)$$

where K_{NP} and K_{ND} represent the normal proportional and derivative gains respectively, E_{Nr} and V_{Nr} are respectively the normal errors and velocities magnitudes related to the bead, α and β are the angles between the x-axis and E_{Nr} and V_{Nr} vectors. In terms of coding, there are eight cases to consider for both angles depending on the orientation segment, error and velocity vectors. The angle θ from Eq. 10 is defined as

$$\theta = \tan^{-1}\left(\frac{z_D - z(t)}{x_D - x(t)}\right) \qquad (12)$$

To ensure that the commands applied do not exceed the gradient limits subdued to each axis, a linear normalization is applied.

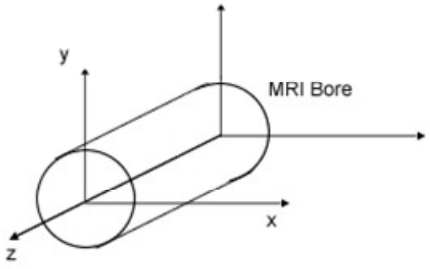

Fig. 1. Axis convention in the MRI environment.

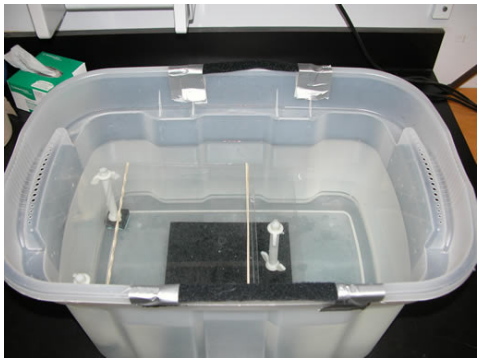

Figure 2: Experimental setup

IV. Results

The tests were conducted with a chrome steel bead of 1.5 mm in diameter whose saturation magnetization is 1.35×10^{-6} A/m. A 1.5 T Siemens Avanto clinical MRI system was used for the experimental tests. The maximum peak-to-peak magnetic gradient amplitude was set to 52 mT/m along the three Cartesian coordinates. A PID controller, whose block diagram in shown in Fig. 3, was used in order to guide and place the bead at specific locations in a PMMA phantom filled up with water and placed in the MRI bore as depicted in Fig. 2. Its density ρ_f is 1 g/cm^3 and its viscosity μ is 0.001002 Pa.s. To maximize the speed of the bead, the spacing between the plates of the phantom were set at 3 mm, i.e. at twice the diameter of the bead. The single echo 3D real-time tracking sequence [6] requires a feedback time $t_{feedback}$ = 30 ms and t_{adc}= 3.84 ms in order to execute properly the tracking, the control, and the propulsion tasks. Based on such constraints for the MRI sequences, the sampling period $h = t_{feedback} - t_{adc}$= 26.2 ms. The time necessary to apply the gradients in order to acquire the 3D dynamic position of the bead [5] t_{gpos} is 15.3 ms.

Consequently, the remaining time available to apply the propulsion gradients is $t_{gprop} = t_{feedback} - t_{gpos} = 14.7$ ms. The time delay between the acquisition of the position information in x and z, d_{xz} is 6 ms. The compensator gains were adjusted heuristically in order to keep the overshoot and steady-state error minimal [9,10]. The simulation data were generated using MATLAB/SIMULINK software. Figures 4, 5 and 6 show the trajectory of the bead obtained experimentally and by simulation for a 2D control experiment along the x and z axes.

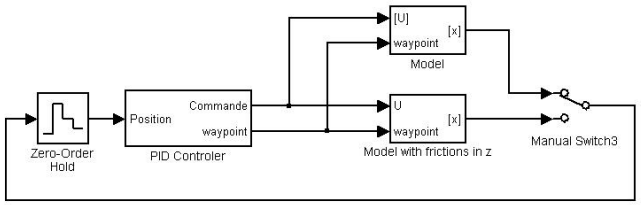

Fig. 3. Block diagram of the discrete closed loop control system

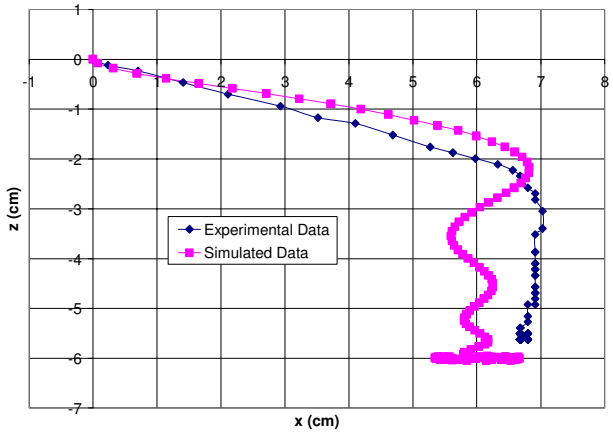

Fig. 4. Plots of the 2D experimental and simulated trajectory of a chrome steel bead of 1.5 mm in diameter along a horizontal plane, in a quiescent flow acquired with a PID controller with $K_{TP} = 0.4$, $K_{TD} = 0.2$, $K_{TI} = 0.2$, $K_{NP} = 0$, $K_{ND} = 0$, where the target coordinates are x = 6 cm and z = -6 cm.

V. Discussion

The 2D control experiments are conducted on a plate instead of a tube in order to evaluate the efficiency of the controller for maintaining a rectilinear motion along each of the segments specified by a roadmap. In Fig. 4, although the target coordinates are equal in magnitude, the bead reaches the assigned coordinate along the x-axis before the one along the z-axis. This is explained by the fact the bead rolls along the x-axis and slides along the z-axis due to the orientation of the DC magnetic field [4]. Hence, the forces of friction along the z-axis are much higher than those along the x-axis. In the simulation, μ_s and μ_k were respectively set to 0.5 and 0.4 [11]. Since the forces of friction due to rolling are negligible, they were not considered in the simulation. In order to overcome the forces of friction along the z-axis, constant upward magnetic gradients of 26 mT/m in amplitude were applied. Fig. 2 shows a good correlation between simulated and experimental data which proves the validity of the model.

Figures 5 and 6 show respectively the simulated trajectory of a bead moving in water against and with a flow of speed $v_f = 5$ cm/s with one intermediate waypoint. The control system is designed in such a way that as soon as the bead enters a zone of diameter $d_z = d_t - r_b$, the target is assigned to the next waypoint. Fig. 5 depicts the positive contribution of the gain K_N which, if not considered, prevents the bead to follow the next segment inclination.

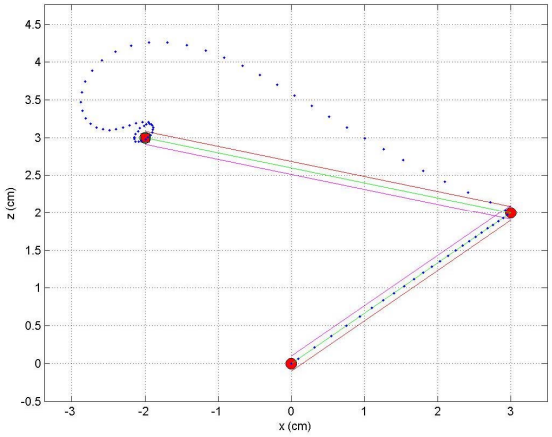

Fig. 5. Plots of the 2D simulated trajectory along the x and z axes of a chrome steel bead of 1.5 mm in diameter along a horizontal duct of 3 mm in width with $v_f = 5$ cm/s, acquired with a PID controller whose gains are with $K_{TP} = 0.4$, $K_{TD} = 0.2$, $K_{TI} = 0.2$, $K_{NP} = 0$, $K_{ND} = 0$, where the destination coordinates are x = -2 cm and z = 3 cm, and the intermediate waypoint coordinates are x = 3 cm and z = 2 cm.

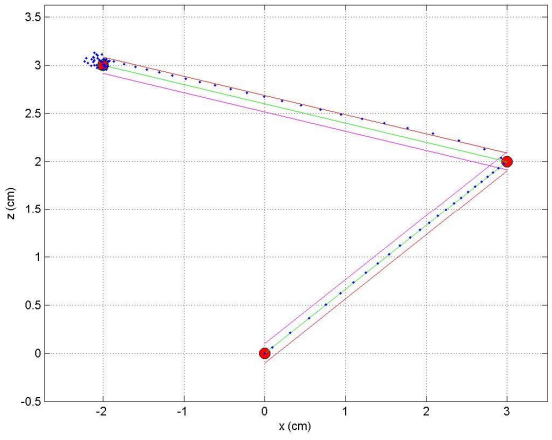

Fig. 6. Plots of the 2D simulated trajectory along the x and z axes of a chrome steel bead of 1.5 mm in diameter along a horizontal duct of 3 mm in width, with $v_f = 5$ cm/s with acquired with a PID controller whose gains are with $K_{TP} = 0.4$, $K_{TD} = 0.2$, $K_{TI} = 0.2$, $K_{NP} = -3$, $K_{ND} = 0.2$, where the final waypoint coordinates are x = -2 cm and z = 3 cm, and the intermediate waypoint coordinates are x = 3 cm and z = 2 cm.

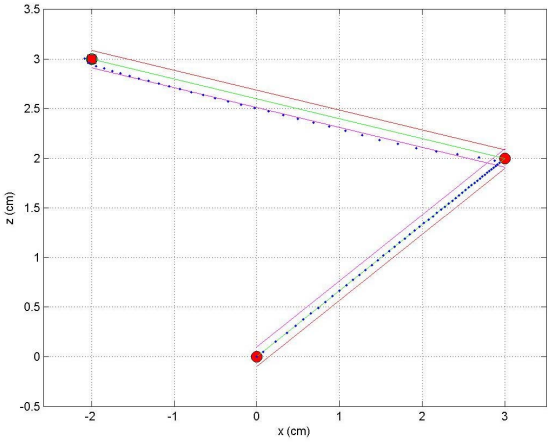

Fig. 7. Plots of the 2D simulated trajectory along the x and z axes of a chrome steel bead of 1.5 mm in diameter along a horizontal duct of 3 mm in width, with vf = -5 cm/s with acquired with a PID controller whose gains are K_{TP} = 0.4, K_{TD} = 0.2, K_{TI} = 0.2, K_{NP} = -3, K_{ND} = 0.2, where the final waypoint coordinates are x = -2 cm and z = 3 cm, and the intermediate waypoint coordinates are x = 3 cm and z = 2 cm.

VI. Conclusion

Results obtained show the validity of the PID as an appropriate controller to investigate and identify the obstacles of the model and to provide adequate adjustments. Future studies will involve pulsating flow as encountered in real blood vessels. As a subsequent step, a 3D *in vitro* control will be carried inside a realistic phantom artery system using a blood analog fluid prior to further tests performed *in vivo*.

Acknowledgment

This project is supported in part by a Canada Research Chair (CRC) in Micro/Nanosystem Development, Fabrication and Validation, the Canada Foundation for Innovation (CFI), the National Sciences and Engineering Research Council of Canada (NSERC), and the Government of Québec. We acknowledge the support of Hôpital Notre-Dame and Centre Hospitalier de l'Université de Montréal (CHUM) that provides the infrastructure to conduct MRI tests. The authors would like to thank particularly Jean-Baptiste Mathieu for the design and the construction of the phantom, as well as Ouajdi Felfoul, Arnaud Chanu, Eric Aboussouan, and Pascal Hannoyer for their suggestions, their support and their readiness in information supply, Professor David Menard for providing the facilities in order to measure the magnetisation of the ferromagnetic beads, and Louis-Philippe Carignan, for his help in the measurements.

References

[1] Mathieu, J.-B., Martel, S., Yahia, L., Soulez, G., and Beaudoin, G., "Preliminary Studies for Using Magnetic Resonance Imaging Systems as a Mean of Propulsion for Microrobots in Blood Vessels and Evaluation of Ferromagnetic Artefacts," *CCECE 2003 Canadian Conference on Electrical and Computer Engineering: Toward a Caring and Humane Technology, May 4-7 2003,* pp. 835-838, 2003.

[2] Mathieu, J.-B., Beaudoin, G., and Martel, S., Method of propulsion of a ferromagnetic core in the cardiovascular system through magnetic gradients generated by an MRI system *Biomedical Engineering, IEEE Transactions on*, vol. 53, no. 2, pp. 292-299, 2006.

[3] Mathieu, J.-B., Martel, S., Yahia, L., Soulez, G., and Beaudoin, G., "MRI Systems as a Mean of Propulsion for a Microdevice in Blood Vessels ," *IEEE Engineering in Medicine and Biology Society ,* Cancun , pp. 3419-3422, Sept. 2003.

[4] Mathieu, J.-B., Martel, S., Yahia, L., Soulez, G., and Beaudoin, G., Preliminary investigation of the feasibility of magnetic propulsion for future microdevices in blood vessels *Bio-Medical Materials and Engineering*, vol. 15, no. 5, pp. 367-374, 2005. 0959-2989.

[5] Aboussouan, A. and Martel, S., "Convolutive tracking for high-precision absolute positioning of medical instruments in MRI," *Engineering in Medicine and Biology Society, 2006. IEEE-EMBS 2006. 28th Annual International Conference of the,* 2006.

[6] Chanu, A., Aboussouan, E., Tamaz, S., and Martel, S., "Sequence design and software environment for real-time navigation of a wireless ferromagnetic device using MRI system and single echo 3D tracking," *Engineering in Medicine and Biology Society, 2006. IEEE-EMBS 2005. 28th Annual International Conference of the,* accepted for publication, 2006.

[7] Sabra, W., Khouzam, M., Chanu, A., and Martel, S., "Use of 3D Potential Field and an Enhanced Breadth-first Search Algorithms for the Path Planning of Microdevices Propelled in the Cardiovascular System," *Engineering in Medicine and Biology Society, 2005. IEEE-EMBS 2005. 27th Annual International Conference of the,* pp. 3916-3920, 2005.

[8] Tamaz, S. and Martel, S., "Impact of the MRI-based Navigation System Constraints on the Step Response Using a PID Controller," *Engineering in Medicine and Biology Society, 2005. IEEE-EMBS 2005. 27th Annual International Conference of the,* pp. 5073-5076, 2005.

[9] O'Dwyer, A. *Handbook of PI and PID controller tuning rules*, New Jersey: World Scientific, 2003.

[10] Ogata, K. *Modern control engineering*, Upper Saddle River, N.J.: Prentice-Hall, 2002.

[11] Dominighaus, H. *Plastics for engineers: materials, properties, applications*, Munich, Allemagne: Hanser Publishiers, 1993.